AGU PUBLICATIONS

JGR

Journal of Geophysical Research: Oceans

RESEARCH ARTICLE

10.1002/2017JC013425

Deep Bering Sea Circulation and Variability, 2001–2016, From Argo Data

Gregory C. Johnson[1] **and Phyllis J. Stabeno**[1]

[1]NOAA/Pacific Marine Environmental Laboratory, Seattle, WA, USA

Key Points:
- Argo salinity, temperature, and velocity data detail deep Bering Sea mean circulation and relation to water mass property distributions
- Relatively warm North Pacific waters enter from the south, cool in a 4–16 Sverdrup cyclonic gyre, and exit through the Kamchatka Strait
- Interannual temperature variations and a -0.006 g kg yr^{-1} freshening trend are prominent in the upper water column of the deep Bering Sea

Correspondence to:
G. C. Johnson,
gregory.c.johnson@noaa.gov

Citation:
Johnson, G. C., & Stabeno, P. J. (2017). Deep Bering Sea circulation and variability, 2001–2016, from Argo data. *Journal of Geophysical Research: Oceans*, *122*, 9765–9779. https://doi.org/10.1002/2017JC013425

Received 1 SEP 2017
Accepted 22 NOV 2017
Accepted article online 30 NOV 2017
Published online 11 DEC 2017

Abstract The mean structure, seasonal cycle, and interannual variability of temperature and salinity are analyzed in the deep Bering Sea basin using Argo profile data collected from 2001 to 2016. Gyre transports are estimated using geostrophic stream function maps of Argo profile data referenced to a 1,000 dbar nondivergent absolute velocity stream function mapped from Argo parking pressure displacement data. Relatively warm and salty water from the North Pacific enters the basin through the Near Strait and passages between Aleutian Islands to the east. This water then flows in a cyclonic (counterclockwise) direction around the region, cooling (and freshening) along its path. Aleutian North Slope Current transports from 0 to 1,890 dbar are estimated at 3–6 Sverdrups (1 Sv $= 10^6$ m^3 s^{-1}) eastward, feeding into the northwestward Bering Slope Current with transports of mostly 5–6 Sv. The Kamchatka Current has transports of ~6 Sv north of Shirshov Ridge, increasing to 14–16 Sv south of the ridge, where it is augmented by westward flow from Near Strait. Temperature exhibits strong interannual variations in the upper ocean, with warm periods in 2004–2005 and 2015–2016, and cold periods around 2009 and 2012. In contrast, upper ocean salinity generally decreases from 2001 to 2016. As a result of this salinity decrease, the density of the subsurface temperature minimum decreased over this time period, despite more interannual variability in the minimum temperature value. The subsurface temperature maximum also exhibits interannual variability, but with values generally warmer than those previously reported for the 1970s and 1980s.

1. Introduction

The deep Bering Sea basin (Figure 1; as opposed to the Bering Shelf) is partially separated from the rest of the North Pacific by the Aleutian and Commander islands. With an abyssal plain ranging from 3,600 to 4,000 m depth, it is actually split into three deep basins. The largest basin is the Aleutian Basin. The Bowers Bank defines the perimeter of the smaller Bowers Basin in the south-central portion of the deep Bering Sea, and the Shirshov Ridge delineates the eastern edge of the smaller Komandor Basin in the west. There are multiple straits and passes that allow water to flow between the North Pacific and the deep Bering Sea basin (Stabeno et al., 2005). The deepest and westernmost of these is Kamchatka Strait, with a sill depth of more than 3,500 m. Near Strait is the next deepest, with a sill depth exceeding 1,800 m, and then comes Amchitka Pass, with a sill depth exceeding 1,000 m.

Mean wind stress curl over the deep Bering Sea basin is positive (Bond et al., 1994), which drives Ekman suction (upwelling), and hence a cyclonic (counterclockwise) circulation there. Long-term mean surface heat flux is out of the ocean and long-term mean surface freshwater flux is into the ocean over the basin (e.g., Large & Yeager, 2009). Hence, to maintain steady state temperature and salinity distributions, relatively warm and salty water must enter the basin from the North Pacific and relatively cold and fresh water must exit the basin into the North Pacific. While cold fresh water also flows into the Arctic through the Bering Strait to the north (Woodgate et al., 2012), much of that water probably transits along the Bering Shelf slope and over the much shallower Bering Shelf, to the east of the deep Bering Sea basin (Panteleev et al., 2011).

Salinity increases from the surface downward in the deep Bering Sea basin year-round, so the vertical salinity gradient contributes positively to the vertical density gradient throughout the water column. Salinity also plays the dominant role in setting the vertical density gradient at least down to 2,000 m, with temperature playing a secondary role except in the seasonal thermocline. However, temperature has a more complicated vertical structure than salinity, with a subsurface temperature minimum (the Θ-min or dichothermal

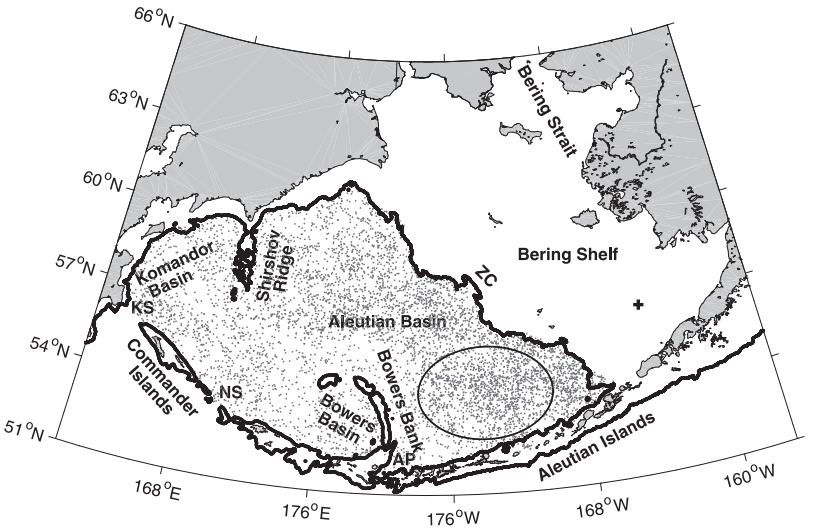

Figure 1. Argo floats (grey dots), southeast deep Bering Sea basin time series analysis region (thin black ellipse), and BS-2 mooring (plus sign) with the 1,000 m isobath (thick black line) and place names (text). Here KS signifies Kamchatka Strait, NS Near Strait, AP Amchitka Pass, and ZC Zhemchug Canyon.

layer), created by winter-time cooling of the mixed layer, present in all but late winter when it is directly connected to the surface (Ueno & Yasuda, 2000). Just below the Θ-min is a subsurface temperature maximum (the Θ-max or mesothermal layer) maintained by inflow of relatively warm, salty, nutrient-rich water from the North Pacific (Reed, 1995).

Temperature, salinity, and velocity within the deep Bering Sea basin have historically been relatively undersampled (Cokelet et al., 1996; Reed et al., 1993), especially in winter, when weather is inclement and seas rough. From June 2001 through December 2016, 69 Argo floats either deployed in or entering into the basin from the North Pacific have collected over 6,000 high-quality CTD (conductivity-temperature-depth) instrument profiles, as well as providing position measurements, which afford an estimate of parking-depth velocities, year-round, sampling the entire basin. Previous regional studies using Argo data over a decade ago had only a small subset of this data set to work with, and thus were limited to relatively short time periods (Wirts & Johnson, 2005) and only portions of the basin (Johnson et al., 2004). Here we use the 2001–2016 Argo data with their expanded spatial and temporal coverage, to study the mean distribution, seasonal cycle, and interannual variations of temperature and salinity over more than 15 years, as well as to quantify the mean circulation for the entire deep Bering Sea basin.

2. Data and Methods

We downloaded Argo profile data, both delayed-mode and real-time quality controlled, from an Argo Global Data Assembly Center (GDAC; http://www.usgodae.org/argo/argo.html) in January 2017 (http://doi.org/10.17882/42182#47708). We used only data flagged 1 (good) for the analysis. Within the deep Bering Sea basin this totaled 6,198 profiles. We also analyzed 4,135 parking depth displacements nominally at 1,000 dbar from 56 of these floats, collected between June 2001 and April 2017. We used updates (http://apdrc.soest.hawaii.edu/projects/yomaha/) of the YOMAHA 2007 (Lebedev et al., 2007) product for this purpose, combining data sets downloaded in June 2013, July 2014, December 2014, November 2015, May 2016, July 2016, October 2016, and April 2017, replacing older data with newer when available.

From each profile, we estimated the mixed layer depth, temperature, and salinity following Holte and Talley (2009). We also put the profile data on a regular 2 dbar pressure vertical grid from 0 to 2,000 dbar. To accomplish this vertical gridding, we interpolated practical salinity (S_P) and temperature (T) versus pressure (P) using a shape-preserving piecewise cubic Hermite interpolating polynomial, filling any missing near-surface values with data from the shallowest measurement. Next we calculated potential temperature (θ) values from the interpolated data.

Following the interpolation, we found a S_P value at $\theta = 2°C$ for $p > 1{,}000$ dbar (well below the subsurface temperature-minimum) for each profile that reached sufficiently deep to sample it. For the resulting time series from each float, we interpolated any missing values of this quantity for individual profiles by applying a loess filter (Cleveland & Devlin, 1988) with a 2 month half-power-point to the profiles from that float where data were present. We then calculated the basin mean (34.529 PSS-78) of the S_P values at $\theta = 2°C$ for $p > 1{,}000$ dbar. We adjusted the S_P values for each profile by an offset so that S_P at $\theta = 2°C$ for $p > 1{,}000$ dbar matched that basin mean value. This adjustment was chosen because the deep θ-S_p relation is quite homogenous in the deep Bering Sea basin, allowing precise evaluation of the float salinity data. The mean (and median) of those offsets was 0.000, and the bulk of the profiles (5,950) were adjusted by less than 0.01, the Argo target for salinity accuracy. However, the standard deviation of the adjustments was ± 0.007, and 105 profiles from three floats were adjusted by more than 0.02, twice the threshold for Argo accuracy. The larger adjustments were generally made to salinity data that had not yet undergone delayed mode scientific quality control. We then calculated the absolute salinity (S_A), conservative temperature (Θ), and potential density anomaly referenced to the surface (σ_0) from T and the adjusted S_P values using TEOS-10 (IOC SCOR & IAPSO, 2010) version 3.05.

Next we interpolated S_A, Θ, and P for each profile onto a σ_0 grid, sorting σ_0 so it was monotonically increasing with increasing pressure (e.g., Thorpe, 1977), but not sorting the other quantities. Then we recalculated σ_0 using the interpolated values of S_A and Θ. If the magnitude of the difference of any of the recalculated and original σ_0 values in a profile exceed 0.1 kg m^{-3} for $\sigma_0 < 26.7$ kg m^{-3} (in the upper ocean) or exceeded 0.006 kg m^{-3} for $\sigma_0 > 26.7$ kg m^{-3} (in the deeper ocean), that profile was discarded from the analysis. These threshold values were determined by visual inspection, which confirmed that this quality control step removed 38 profiles from 18 floats with substantial density inversions (Figure 2; black lines). Of the remaining 6,160 profiles (Figure 2 grey lines; Figure 1, dots), 3,498 reached 1,890 dbar, 5,481 reached 990 dbar, and 6,084 reached 490 dbar. We chose those pressures because many profiles fall somewhat shy of their nominal target maximum pressures (e.g., 2,000, 1,000, and 500 dbar) owing to float programming.

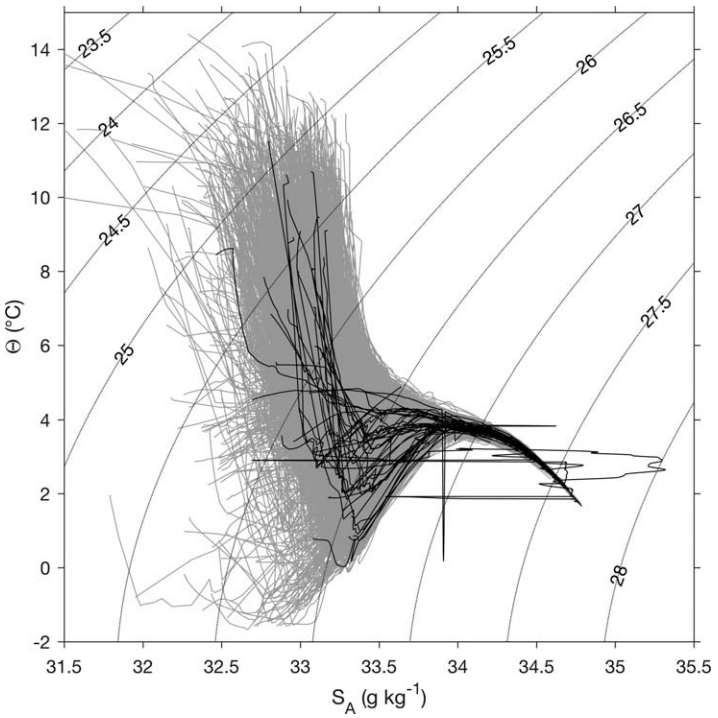

Figure 2. Conservative temperature-absolute salinity (Θ-S_A) plots of the 6,160 deep Bering Sea basin float data profiles used in this study (grey lines) and the 38 discarded prior to analysis (black lines) using a quality control procedure described in section 2. Potential density surfaces (dotted labeled contours) are overlain.

We used parking velocity estimates from updates of YoMaHa'07 (Lebedev et al., 2007). These parking velocities were estimated as differences of the first position fix from the most recent profile and the last position fix from the previous profile. The locations of the velocity estimates were assumed to be the mean locations of each pair of positions fixes. If either position fix in the pair used in estimating the displacement was associated with a water depth shallower than 1,000 m based on ETOP01 (Amante & Eakins, 2009) bathymetry, we discarded that displacement vector. We visually inspected the remaining data and found no obvious outliers, so we used the remaining data.

We mapped the spatial mean distributions of the average of Θ and S_A over 0–490 dbar and the geostrophic transport stream function Q/f_o integrated over 0–990 dbar as well as over 990–1,890 dbar, where f_o is the Coriolis parameter at 56.5°N and Q is the double vertical integral of the dynamic height in the relevant vertical direction from 990 dbar to both 0 and 1,890 dbar. To do these analyses, we first fit a spatial plane (a least squares fit of a mean value and linear functions of latitude and longitude), annual, and semiannual harmonics to the profile values and removed those fits from the values for each profile for all parameters. We then mapped the residuals using a loess filter with length scales of 4° longitude and 1.6° latitude, adding the spatial planar fit (but not the harmonics) back in for the final maps. We also mapped the velocity stream function at the 1,000 dbar parking depth using the individual displacement data. For that purpose, we used an objective mapping that enforces nondivergence (Bretherton et al., 1976; Gille, 2003) assuming a Gaussian covariance function for the stream function with length scales of 5° longitude, 2.75° latitude (both roughly 305 km at 56.5°N), and a noise-to-signal ratio of unity. The

resulting zonal velocity covariance function has a meridional zero crossing at ~215 km and its largest negative values at ~375 km. The zonal-meridional velocity covariance magnitudes are zero along the zonal and meridional axes, peaking in each quadrant at ~305 km radial distance. In all cases, maps were constructed on a 1/4° longitude by 1/8° latitude grid in the deep Bering Sea, estimating values at grid points where the averaged depth exceeded either 1,000 or 2,000 m, as appropriate.

We chose 0–490 dbar for the vertically averaged Θ and S_A analysis because a large number of floats sample to that pressure, and this pressure range encompasses the great bulk of the variability in the temperature profiles. About 99% of the pressure-integrated temperature variance from 0 to 2,000 dbar is found from 0 to 490 dbar. Salinity variability extends deeper than temperature variability partly because salinity plays a dominant role in the vertical stratification, and so reflects a larger proportion of the vertical isopycnal excursions linked to currents eddies, internal waves, and internal tides. Because these excursions extend into the deep ocean, especially in subpolar regions, only 90% of the pressure-integrated salinity variance from 0 to 2,000 dbar is found from 0 to 490 dbar. We chose 0–990 dbar and 990–1,890 dbar for the transport stream function analyses because 990 dbar is very close to the 1,000 dbar nominal park pressure for the majority of the floats, but allows inclusion of more profiles compared to 1,000 dbar, as does 1,890 dbar (as opposed to 1,900 or 2,000 dbar).

We also constructed time series of mixed-layer properties, as well as Θ and S_A versus pressure by averaging values every 1/4 month within a 1 month running window using data found within a particularly well-sampled ellipse of radii 4° longitude and 1.6° latitude centered at 174°W, 54.5°N (Figure 1, thin black line). We required at least three data points within that ellipse to compute averages at each time bin, and as a result averages for some time periods were missing from that time series.

Finally, we compared some of our Argo profile analysis to vertically averaged temperature data from the BS-2 mooring (Stabeno et al., 2012; https://www.pmel.noaa.gov/foci/foci_moorings/mooring_info/mooring_location_info.html) which is located in 71 m of water at 56.869°N, 164.050°W on the Bering Shelf (Figure 1, plus sign). We used BS-2 mooring annual averages from 2001 to 2016, excluding 2010 and 2014, when moorings were lost.

3. Results

We first present analyses of the seasonal cycle of Θ and S_A averaged from the surface to 490 dbar. After removing those seasonal cycles, we analyze the mean spatial patterns for those quantities. Analysis of mean circulation in the deep Bering Sea basin comes next, and its relation to the mean spatial patterns of pressure-averaged upper ocean Θ and S_A. We follow with presentations of interannual variations of pressure-averaged Θ and S_A on a basin-scale (with the mean seasonal cycle and spatial patterns removed), and temporal variations (including both seasonal and interannual signals) as a function of pressure for a time series constructed in the Aleutian Basin.

3.1. Seasonal Cycle of Θ and S_A

The basin-scale seasonal cycle of Θ averaged from the surface to 490 dbar (Figure 3a), with a spatial planar fit removed, approaches a minimum of 3.1°C in late March, and a maximum of 4.0°C in late September. This range of nearly 0.9°C is about three times the standard deviation of the residuals of the fit, which is about 0.3°C. Some of this residual is spatial variability that is not explained by the crude spatial planar fit, and some is variability on both shorter (subseasonal, e.g., eddies, waves, internal tides, etc.) and longer (interannual to decadal) timescales.

The seasonal cycle of S_A averaged from the surface to 490 dbar, again with a planar spatial fit removed (Figure 3b), exceeds 33.71 g kg^{-1} at the start of February, and dips below 33.63 g kg^{-1} at the end of September. The seasonal range of almost 0.09 g kg^{-1} is less than a third of the standard deviation of the residuals of the fit, which is about 0.3 g kg^{-1}. This large standard deviation is again partly owing to the crude nature of the planar spatial fit, as revealed just below by the mean spatial pattern. Again, because of the large role salinity plays in setting the density, its variance is increased over that of temperature, owing to dynamical signatures such as eddies, fronts, jets, and currents, as well as internal waves and tides.

3.2. Mean Spatial Patterns of Θ and S_A

After removal of the basin-scale seasonal cycle, the mean spatial pattern of Θ averaged from the surface to 490 dbar (Figure 4a) shows warmest waters around the southeastern fringe of the deep Bering Sea basin,

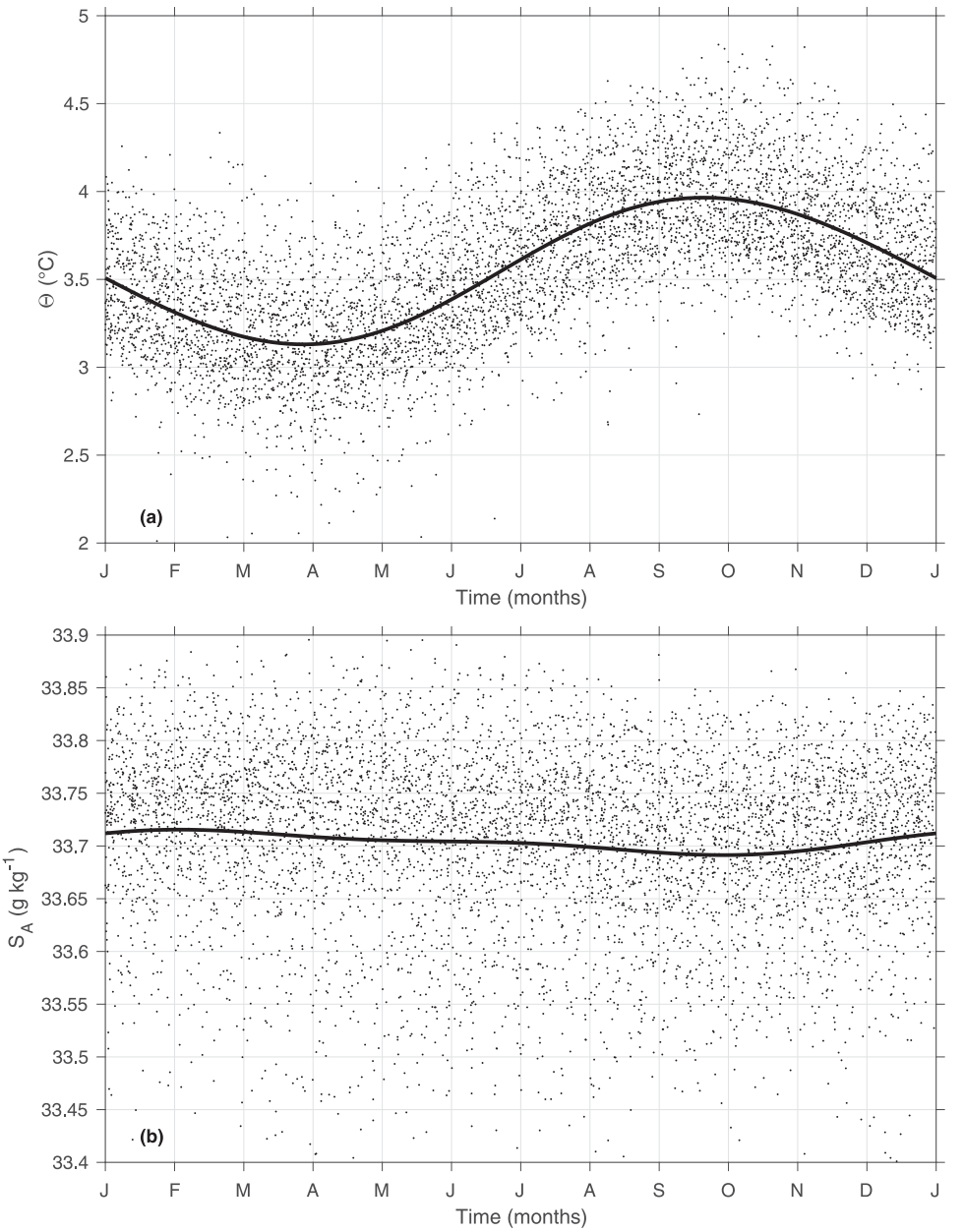

Figure 3. (a) Conservative temperature (Θ, °C) and (b) absolute salinity (S_A, g kg^{-1}) values averaged from 0 to 490 dbar (black dots) for Argo float profiles within the deep Bering Sea basin (Figure 1, black dots) plotted versus time of year (months) with spatial planar fits versus latitude and longitude removed and annual and semiannual harmonics (black lines) simultaneously fit to model the seasonal cycle.

with values exceeding 3.8°C north of the Aleutian Islands starting east of Near Strait, extending counterclockwise (cyclonically) around the basin to just off the Bering Shelf to about 58°N. Mean values exceed 3.4°C west of the entire eastern Bering Shelf, all the way to the apex of the deep Bering Sea near 62°N. The coldest mean values, dipping below 2.4°C, are located south of 60°N in the western end of the basin, just east of Kamchatka, within the Komandor Basin.

After removal of the basin-scale seasonal cycle, the mean spatial pattern of S_A averaged from the surface to 490 dbar (Figure 4b) shows freshest waters around the fringe of the deep Bering Sea basin, and the saltiest waters just north and west of Near Strait. The saltiest mean values exceed 33.85 g kg^{-1} and the freshest mean values dip below 33.50 g kg^{-1} east of Kamchatka. This range of 0.35 g kg^{-1} is comparable to the

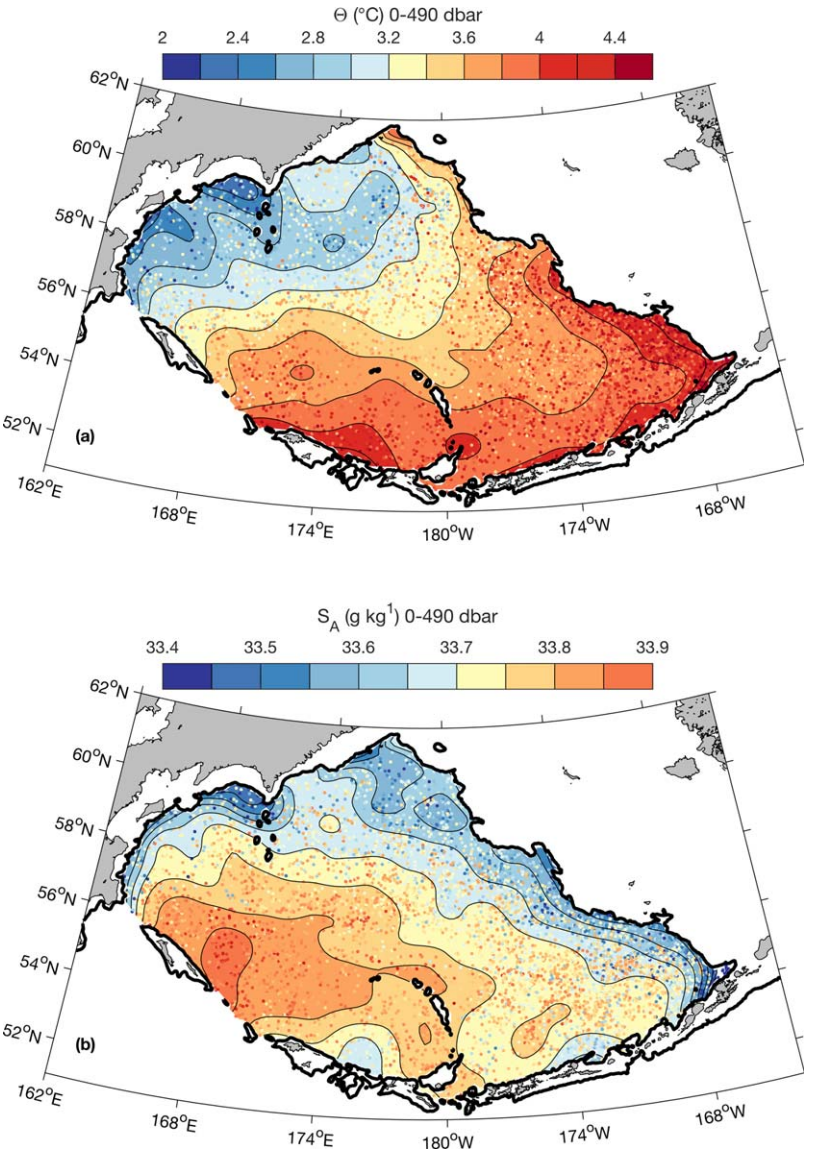

Figure 4. (a) Conservative temperature (Θ, °C) and (b) absolute salinity (S_A, g kg^{-1}) values averaged from 0 to 490 dbar (colored dots) for Argo float profiles within the deep Bering Sea basin (Figure 1, black dots) with seasonal cycles (Figure 3, thick black lines) removed. Data are mapped with a loess filter with length scales of 4° longitude and 1.6° latitude and contoured at 0.2°C intervals for Θ and 0.05 g kg^{-1} intervals for S_A (colored contours, see legends).

residual of the initial fit described above, and clearly a planar spatial model does not capture much of the spatial structure of the mean distribution.

3.3. Mean Circulation

The transport stream function, Q/f_o, for 0–990 dbar relative to an assumed zero velocity at 990 dbar (Figure 5a), suggests an inflow of about 3 Sverdrups (1 Sv = 10^6 m^3 s^{-1}) through the Near Strait and an outflow of about 4–5 Sv through the Kamchatka Strait, with a minimum to the north of the Commander Islands and maxima around the periphery of the rest of the deep Bering Sea basin. The differences of this interior minimum and the peripheral maxima range from about 2 to 7 Sv, so the average magnitude of the cyclonic gyre within the basin is around 3–4 Sv, assuming the velocity at 990 dbar is zero.

However, the mean velocity at 990 dbar is not zero, but instead also exhibits a general cyclonic tendency around the deep Bering Sea basin. Appling a nondivergent stream-function map of the mean velocity at 1,000 dbar (again using the value of f_o at 56.5°N) to the 0–990 dbar transport stream function referenced to

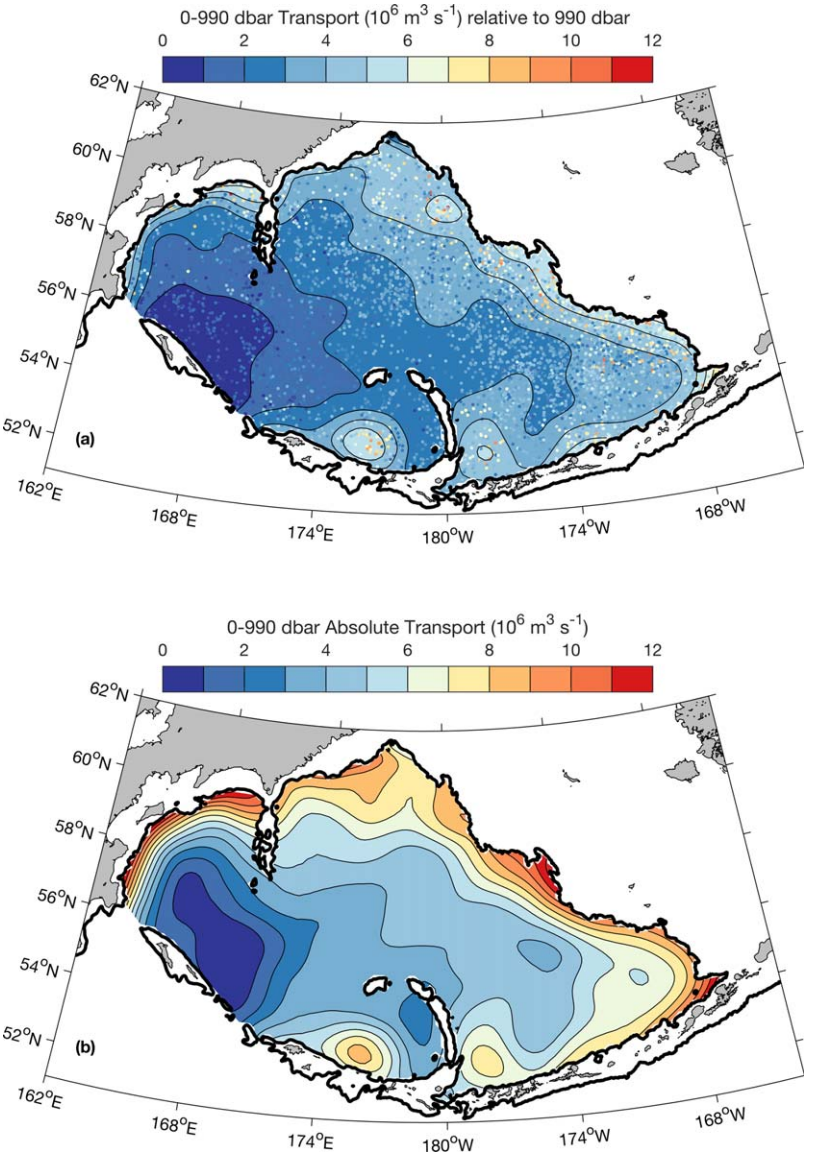

Figure 5. (a) Transport stream function (Q/f_o, 10^6 m^3 s^{-1}) values from 0 to 990 dbar relative to 990 dbar (colored dots) for Argo float profiles within the deep Bering Sea basin (Figure 1, black dots) with seasonal cycle removed. Data are mapped with loess filter with length scales of 4° longitude and 1.6° latitude and contoured at 1 × 10^6 m^3 s^{-1} intervals (colored contours, see legend). (b) Absolute transport stream function for 0–990 dbar (10^6 m^3 s^{-1}) constructed by adding map in Figure 5a to 0–990 dbar transport owing to 1,000 dbar velocities mapped using an objective mapping that enforces non-divergence (Bretherton et al., 1976; Gille, 2003) assuming a Gaussian covariance function with length scales of 5° longitude, 2.75° latitude, and a noise-to-signal ratio of unity. Contoured at 1 × 10^6 m^3 s^{-1} intervals (colored contours, see legends). All values offset by the minimum mapped value in each plot.

zero velocity 990 dbar results in an absolute velocity referenced stream function from 0 to 990 dbar (Figure 5b). This transport stream function map suggests an inflow of about 5 Sv northward through Near Strait into the basin and an outflow southward through the Kamchatka Strait as large as 11 Sv. These numbers are not inconsistent as substantial inflows of North Pacific water are known to occur through Amchitka and Amukta passes to the east, with lesser inflows through the shallower passes still further east (Stabeno et al., 2005). Values of the 0–990 dbar absolute transport around the rest of the border of the basin range from 4 to 12 Sv, generally increasing cyclonically from a minimum value west of Near Strait.

A similar procedure can be applied to estimate the transport stream function from 0 to 1,890 dbar (Figure 6), which adds to the magnitude of the cyclonic gyre within the deep Bering Sea basin. The geostrophic transport

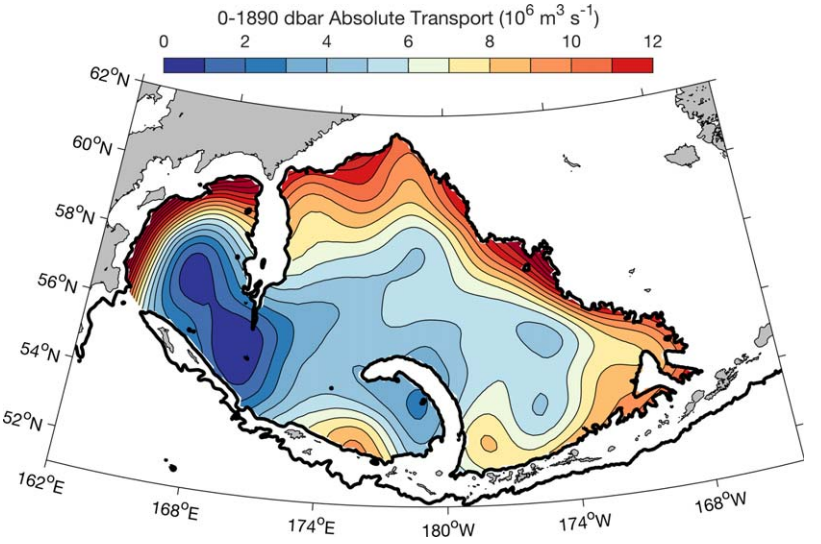

Figure 6. Absolute transport stream function for 0–1,890 dbar (10^6 m^3 s^{-1}) constructed by adding transport stream function (Q/f_o) values integrated from 0 to 1,890 dbar relative to 990 dbar following details in Figure 5a to 0–1,890 dbar transport owing to 1,000 dbar velocities following details in Figure 5b. Contoured at 1 × 10^6 m^3 s^{-1} intervals (colored contours, see legend). All values offset by the minimum mapped value.

stream function from 1,890 to 990 dbar relative to zero at 990 dbar (not shown) displays a slight anticyclonic tendency with a maximum value just west of Near Strait, but it is overwhelmed by the cyclonic tendency of the 1,000 dbar velocity stream function applied to the 1,890–990 dbar layer. The inflow through Near Strait for 0–1,890 dbar absolute velocities is about 6 Sv, and the outflow through Kamchatka Strait could reach as high as 16 Sv. Values around the periphery of the basin excluding those between Kamchatka and Near straits range from 4 to 16 Sv, again generally increasing cyclonically from a minimum value west of Near Strait all the way around to Kamchatka Strait.

3.4. Interannual Variations of Θ and S_A

Interannual variations in Θ averaged from the surface to 490 dbar (Figure 7a) are evident after removal of the seasonal cycle (Figure 3a) and the mean spatial pattern (Figure 4a). Values smoothed with a 1 year loess filter rise from 3.4°C at the start of the record in late 2001 to almost 3.8°C in early 2004, then fall from mid-2005 through 2009, approaching a minimum of 3.3°C. From this minimum, they rise to a maximum exceeding 3.5°C in mid-2011, then fall by about 0.2°C in mid-2012. They rise steadily from mid-2012 through early 2015, then more slowly approach a maximum of 3.9°C near the end of 2016 (also the end of the analysis). Again, the range of interannual variations, about 0.6°C, is roughly three times the 0.2°C standard deviation of the residual. This interannual range is comparable to, although slightly less than, the 0.9°C range of the seasonal cycle.

Variations in S_A averaged from the surface to 490 dbar (Figure 7b) after removal of the basin-scale seasonal cycle (Figure 3b) and the mean spatial pattern (Figure 4b) reveal an overall decadal salinity trend (toward freshening) on the order of −0.006 g kg^{-1} yr^{-1}, with some variations superimposed. As a result of this trend, mean values fall by about 0.09 g kg^{-1} over the 15.6 years of the analysis period. This net freshening value is slightly larger than the standard deviation of the residuals, which is 0.07 g kg^{-1}.

3.5. Time-Vertical Structure of Θ and S_A in the Southeastern Deep Bering Sea

The time series of Θ versus pressure (Figure 8) within an ellipse centered at 174°W, 54.5°N (Figure 1, thin black line), while localized to the southeastern deep Bering Sea basin, is consistent with the seasonal and interannual variations discussed above for the entire region. The surface mixed layer is warmest and shallowest in August, then deepens and cools from August until February and March, respectively. After March, the mixed layer depth shoals rapidly into spring, warming more slowly. Surface mixed layer depths are around 15–20 dbar in August and around 80–160 dbar in February and March. The mean mixed layer depths shown can be considerably less than the maximum mixed layer depths, especially in winter (when

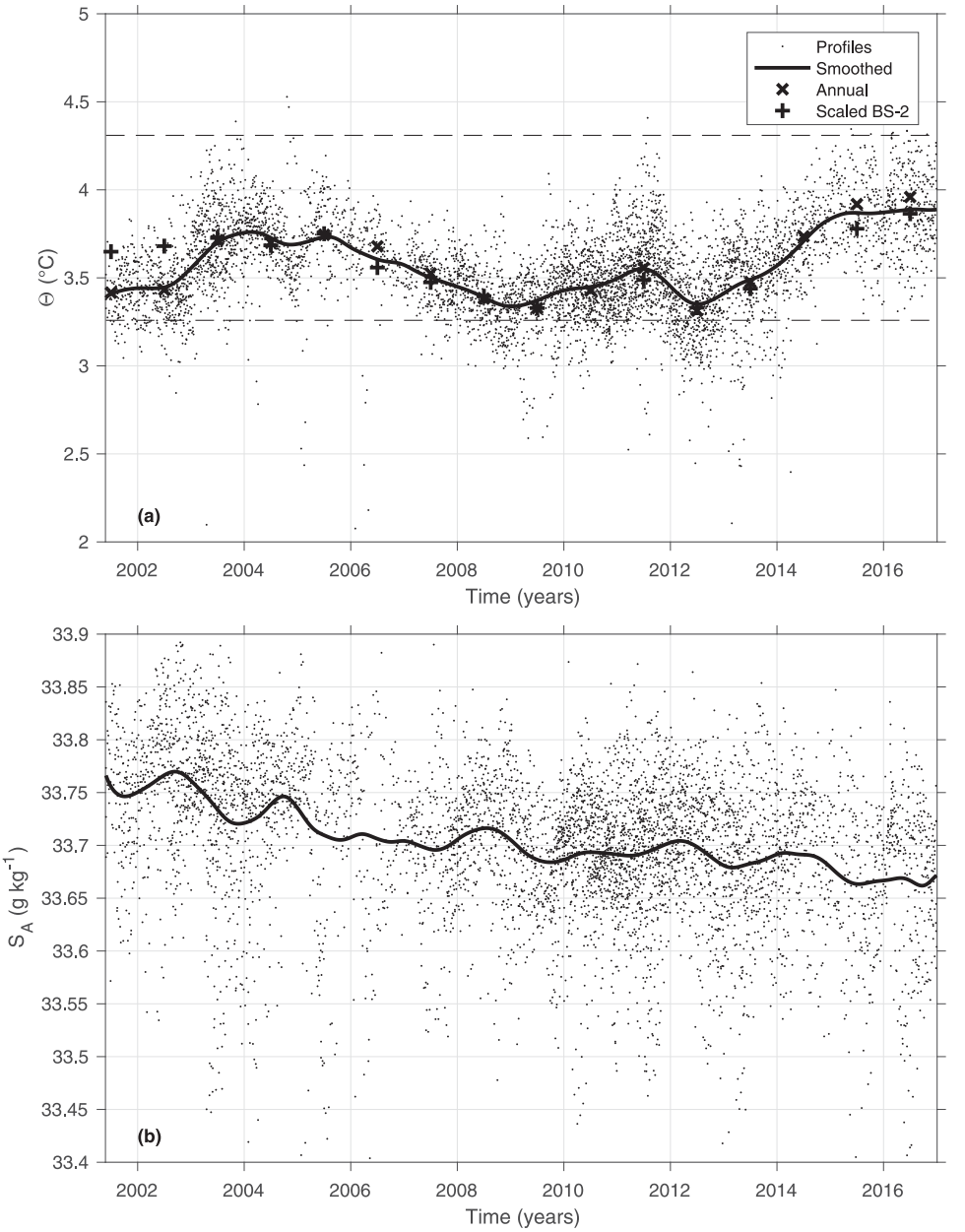

Figure 7. (a) Conservative temperature (Θ, °C) and (b) absolute salinity (S_A, g kg^{-1}) values averaged from 0 to 490 dbar (black dots) for Argo float profiles within the deep Bering Sea basin (Figure 1, black dots) plotted versus time (years) with annual and semiannual harmonics (Figure 3, black lines) as well as the mapped spatial patterns (Figure 4) removed but with the mean values added back in. Data are temporally smoothed with a 1 year loess filter (thick black line). (a) Annual 0–490 dbar Θ averages in the basin (crosses) are correlated at 0.84 with all available annual averages of 0–71 m vertical means (plus signs) at the BS-2 mooring site on the Bering Shelf (Figure 1, plus sign). The BS-2 mooring values have been scaled and shifted for optimal comparison with 0 and 10°C for their scale indicated by the lower and upper horizontal dashed lines, respectively.

values from individual profiles exceed 200 dbar in a few instances). Surface mixed layer temperatures usually peak between 9 and 10°C in August, but do not reach 9°C in 2001, 2009, and 2010, and exceed 10°C in 2005, 2015, and 2016. Mixed layer temperatures usually reach minima between 2.5 and 3.0°C in February, dipping below 2.5°C in 2008, 2010, and 2012, while remaining warmer than 3.0°C in 2002–2006 and 2015. The subsurface temperature maximum, centered at 200–300 dbar is warmest around 2006 and 2016, after relatively warm winters, and weakest in 2002 and 2011 after colder winters.

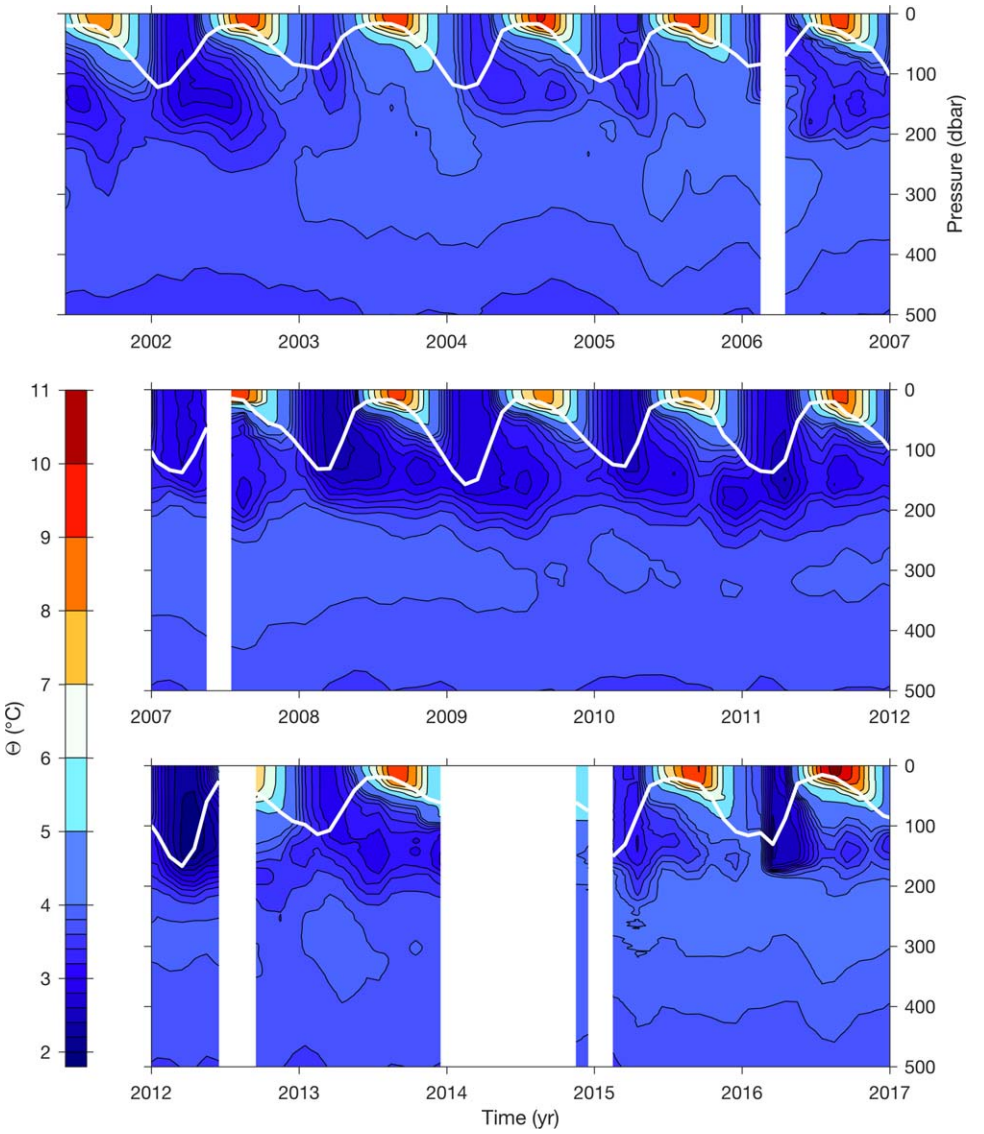

Figure 8. Conservative temperature (Θ,°C) versus pressure (dbar) and time (years) averaged every 1/4 month within a 1 month running window using data found within an ellipse of radii 4° longitude and 1.6° latitude centered at 174°W, 54.5°N (Figure 1, thin black line) contoured at 1°C and 0.2°C intervals above and below 4°C (see color bar). Average mixed layer depths (white line) are also plotted. At least three data points are required within the ellipse to compute averages.

The time series of S_A versus pressure centered around 174°W, 54.5°N (Figure 9) is again consistent with the seasonal and interannual variations discussed above. The permanent halocline found below the maximum depths of the winter mixed layer is augmented by a seasonal halocline in summer, similar to the development of seasonal thermocline in the summer. However, interannual variation in S_A is different in character than for Θ, with freshening apparent over the length of the record in the upper few hundred dbar of the water column.

Average Θ-S_A curves for select years (Figure 10) within the southeast deep Bering Sea basin ellipse (Figure 1, thin black line) illuminate changes in the subsurface temperature minimum (Θ-min) formed in late winter, and the subsurface temperature maximum (Θ-max) below it. The Θ-min is cold, relatively salty (and hence densest at $\sigma_0 = 26.6$ kg m^{-3}) in 2002, and the Θ-max is also cold and dense. By 2005 the subsurface is so warm hardly a Θ-min or a Θ-max is distinguishable. In 2008 and 2012, the Θ-min is colder than in 2002, but also trending fresher, and thus less dense than in 2005. In 2013 and 2016, the Θ-min is of intermediate temperatures, but trending even fresher, and hence lighter (approaching $\sigma_0 = 26.4$ kg m^{-3} in 2016). The Θ-max

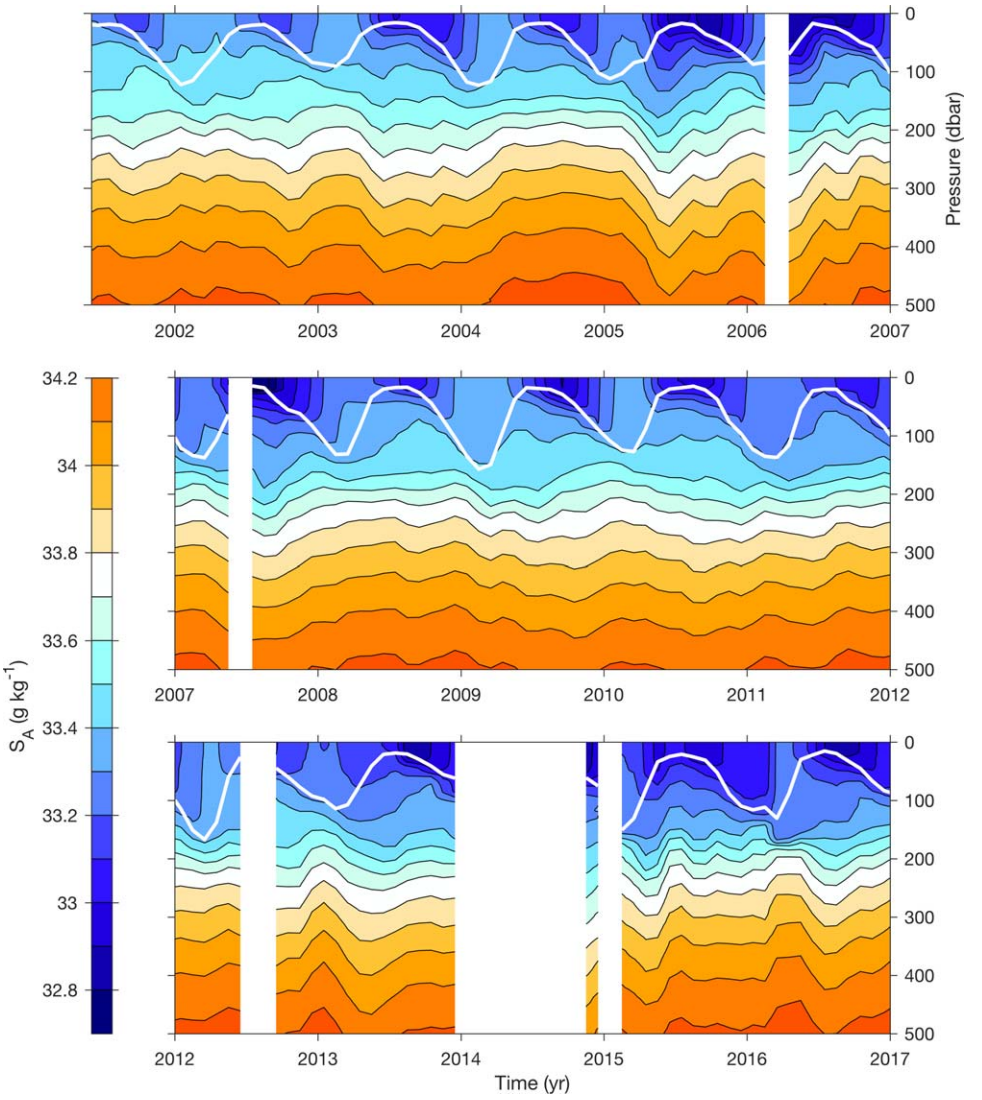

Figure 9. Absolute salinity (S_A, g kg^{-1}) versus pressure (dbar) and time (years) averaged every 1/4 month within a 1 month running window using data found within an ellipse of radii 4° longitude and 1.6° latitude centered at 174°W, 54.5°N (Figure 1, thin black line) contoured at 0.1 g kg^{-1} intervals (see color bar). Average mixed layer depths (white line) are also plotted. At least three data points are required within the ellipse to compute averages.

is even more prominently warm in 2016 (and also light). The freshening (and hence lightening, even in the face of interannual temperature variations) of the Θ-min over the length of the record is prominent.

4. Discussion

The seasonal cycle of Θ averaged from 0 to 490 dbar in the deep Bering Sea basin is substantial and well-defined, with a minimum value approaching 3.1°C in late March and a maximum approaching 4.0°C in mid-September (Figure 3a). During 2001–2016, surface values around 174°W, 54.5°N typically peak at 9–10°C in August and reach minimum values of 2.5–3°C in February, when monthly mean mixed layer depths reach 80–160 dbar, renewing the subsurface temperature minimum (Figure 8). In contrast, the seasonal cycle of S_A averaged from 0 to 490 dbar in the basin (Figure 3b) is slight and does not rise above variability over other time scales, with a hint of a maximum at the start of February and a minimum at the end of September. This faint depth-averaged result is nonetheless consistent with a more apparent seasonal halocline, with fresher water accumulating near the surface in the spring and summer months as

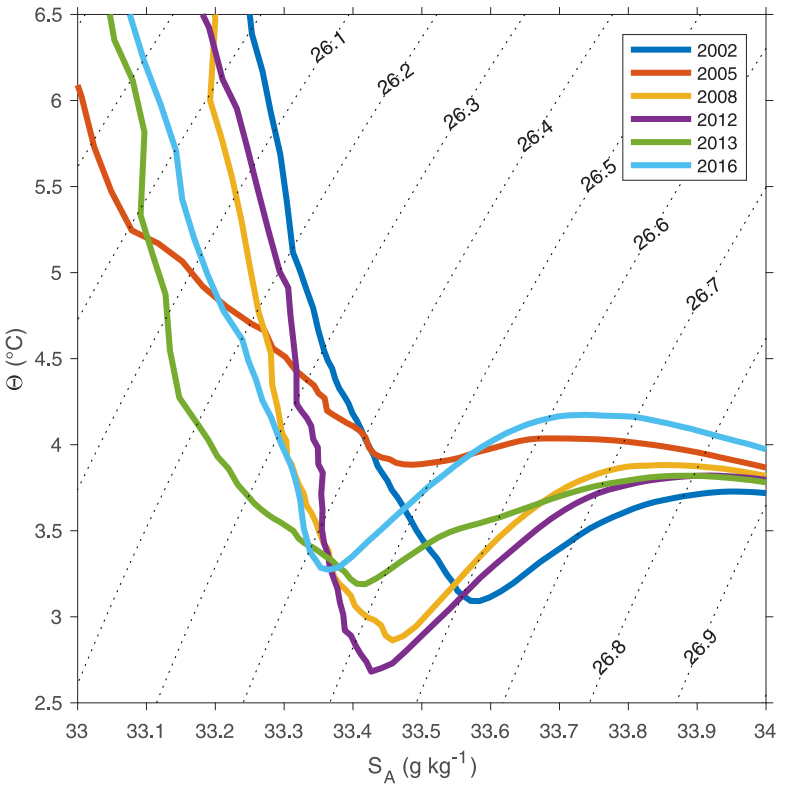

Figure 10. Conservative temperature-absolute salinity (Θ-S_A) plots (colored lines) averaged on potential density surfaces (e.g., dotted labeled contours) using data from all profiles found within an ellipse of radii 4° longitude and 1.6° latitude centered at 174°W, 54.5°N (Figure 1, thin black line) during select years (see legend).

the mixed layer shoals and saltier waters entrained from below in the fall and winter when the surface mixed layer deepens (Figure 9).

With the seasonal cycles removed, the mean spatial patterns of Θ (Figure 4a) and S_A (Figure 4b) averaged from 0 to 490 dbar in the deep Bering Sea basin are closely related to the circulation (Figure 5b) and the surface fluxes of heat and freshwater. Relatively warm and salty North Pacific waters enter the basin from the south through Near Strait. These waters first flow eastward along the north slope of the Aleutian Island Arc in the Aleutian North Slope Current (ANSC). In the east they are augmented by much fresher Alaska Coastal Current water flowing through multiple shallower Aleutian passes. These waters then flow northwestward just west of the Bering Shelf in the Bering Slope Current (BSC), and finally southwestward in the Kamchatka Current (KC) before exiting the basin through the Kamchatka Strait. In the mean, these waters lose heat to the atmosphere and gain freshwater from the atmosphere, ice melt, and land during their cyclonic transit around the basin, so they are warmest and saltiest where they enter from the North Pacific (along the Aleutians from Near Strait to the Alaska Peninsula) and coolest and freshest where they exit (through Kamchatka Strait). Consonant with this assertion, pressure-averaged temperature values are highest just north of the Aleutians to the east of Near Strait and just west of the eastern Bering Shelf, drop west of the northern reaches of the Bering Shelf, and then reach a minimum in the southwest basin, just east of Kamchatka Peninsula.

However, the pressure-averaged salinity pattern (Figure 4b) is more similar to the transport stream function patterns (Figures 5 and 6) than the pressure-averaged temperature pattern (Figure 4a) because salinity is more strongly linked to density (hence the circulation pattern) than temperature in this subpolar region. The uplift of isopycnals in the center of the cyclonic subpolar gyre and the depression in the boundary currents around the edges of the deep Bering Sea basin, coupled with the tight relation between salinity and density in the region means that the 0–490 dbar S_A is highest between Near and Kamchatka straits, where the transport stream function is a minimum, and lowest along the eastern Bering Shelf and Kamchatka,

where the transport stream function is a maximum. It is difficult to distinguish freshening in the transit around the gyre owing to the mean freshwater addition to the basin, especially since the transport stream function also generally increases around the gyre cyclonically from Near Strait to Kamchatka Strait (Figures 5 and 6).

The transport estimates from this analysis reveal the large changes in transport that result when absolute velocities at 1,000 dbar are used to reference geostrophic velocity (Figure 5b) compared to assuming a zero-velocity surface at 990 dbar (Figure 5a). This result is consistent with past studies, for instance two studies analyzing the same data set but assuming a 1,500 dbar level of no-motion in one case (Reed et al., 1993) and using shipboard ADCP data as a reference in the other (Cokelet et al., 1996). Furthermore, the analysis demonstrates that currents persist well below 1,000 dbar, so including deeper portions of the water column in transport estimates increases the magnitude of the cyclonic transport around the deep Bering Sea basin even more (Figure 6). This result is not surprising in the subpolar regions, where the stratification is relatively weak and the Coriolis parameter large, resulting in more depth-independent flows (e.g., Chen & Firing, 2006).

The mean transport maps (Figures 5 and 6) mask considerable mesoscale variability and perhaps structure, that are reflected both in the individual values of transport stream function, Q/f_o, (Figure 5a colored dots) and in the formal error map for the 1,000 m velocity stream function (not shown). The latter is expressed as a fraction of the standard deviation and is dependent on the data distribution as well as the stream function covariance and signal-to-noise ratio used. This formal error has relatively constant values that approach a minimum of 0.31 in the eastern portion of the deep Bering Sea basin where data are most plentiful, and increase slightly to the west and around the rest of the periphery where data are sparser, reaching a maximum of 0.34 near 170°E along the south edge of the basin. Consistent with these indicators, individual float trajectories vary around the mean. For example, 13 floats exit the basin through the Kamchatka Strait, where a strong mean outflow is found in the transport maps, but three floats move through the strait in the opposite direction (http://www.meds-sdmm.dfo-mpo.gc.ca/isdm-gdsi/argo/canadian-products/movies/Bering.avi), reflecting temporal and perhaps even small-scale spatial variations in the flow field.

Individual currents around the deep Bering Sea basin include the ANSC, a narrow, swift eastward flow along the north slope of the Aleutian Islands with an estimated 6 Sv transport. East of Near Strait the ANSC is fed by relatively warm and salty water from the North Pacific flowing northward primarily through Amchitka, Amukta, and Buldir passes between Aleutian Islands (Stabeno et al., 2009). We find the 0–1,890 dbar transport along the Aleutian Islands east of Near Strait to range from 3 to 6 Sv, a bit low of the previous estimate. This discrepancy may be owing partly to the narrowness of the ANSC, which could cause it to be undersampled by the Argo floats. The ANSC is connected to the BSC a wider, eddy-rich, seasonally varying northwestward flow found to the west of the Bering Slope (Ladd, 2014), with a mean transport estimated at 6 Sv by an earlier study using float data (Johnson et al., 2004). The BSC is augmented by fresher Alaska Coastal Current water flowing through the shallower eastern Aleutian passes. For the BSC, the 0–1,890 dbar transport is generally around 5–6 Sv, but with a maximum of about 10 Sv near the Zhemchug Canyon, a location with strong on-shelf flow, but also little float data (Figure 1) near the slope so the mappings may extrapolate overmuch there. The BSC feeds the KC, a subpolar western boundary current with a transport estimated at about 14 Sv near Kamchatka Strait using synoptic data (Cokelet et al., 1996) but as high as 24 Sv using an inverse model (Panteleev et al., 2006). Our estimate of the 0–1,890 dbar KC transport is about 6 Sv northeast of the Shirshov Ridge, and the current is quite wide there. Southwest of the Shirshov Ridge, within the Komandor Basin, the KC is augmented by westward flow originating from Near Strait, the current narrows considerably, and our transport estimate ranges from 14 to 16 Sv.

Interannual variations of upper ocean temperature and salinity in the deep Bering Sea basin have different characters. The upper ocean is warm in 2003–2005 and again in 2013–2016, but cooler in 2002 and 2006–2012 (Figures 7a and 8). Annual averages of mean 0–490 dbar temperatures in the basin (Figure 7a, crosses) are very well correlated ($r = 0.84$) with annual averages of mean 0–71 m mooring temperatures on the Bering Shelf (Figure 7a, plus signs; Stabeno et al., 2012, 2017). In contrast, upper ocean salinity in the basin largely trends fresher at a rate of 0.006 g kg^{-1} yr^{-1} over the 2001–2016 record (Figures 7b and 9). As a result of these variations, the Θ-min is saltiest (and densest) in 2001 and 2002, and freshest (as well as lightest) in 2015 and 2016, with a nearly monotonic salinity progression in the intervening years (Figure 10). However, the Θ-min is actually coldest (but not densest) in 2008–2010, during a relatively cold period, and

warmest in 2005, after a relatively mild winter. The deeper subsurface Θ-max is also least apparent in 2003 and 2005, after warm winters. The Θ-max is coldest and saltiest (hence densest) in 2002 and 2001, and warmest and freshest (hence lightest) in 2015 and 2016. The Θ-max does not exhibit a monotonic increase in temperature or decrease in salinity (although salinity changes are more secular) in the intervening years. However, annual mean subsurface Θ-max values from 2001 to 2016 range from about 3.73 to 4.17°C, generally higher than mean values from 3.60 to 4.06°C reported from surveys in the region for 9 years between 1971 and 1993 (Reed, 1995), suggestive of a long-term subsurface warming in the basin.

Interannual variability in upper ocean temperature and salinity in the southeastern deep Bering Sea basin is driven both by atmospheric forcing (wind stress and air-sea heat and freshwater fluxes) and ocean advection (Wirts & Johnson, 2005). Oceanic variability on the eastern Bering Sea shelf is primarily driven by atmospheric forcing both directly and through ice, but only secondarily to advection of Gulf of Alaska water through eastern passes (Stabeno et al., 2017). Atmospheric and oceanic variability in the region can be related to large-scale North Pacific sea level pressure variations (Overland et al., 2012).

The decadal freshening trend in the upper few hundred dbar of the deep Bering Sea basin (Figures 7b, 9, and 10) is in broad agreement with trends from 1950–2008, which show freshening in the high latitude Pacific, consistent with an amplification of the global hydrological cycle (Durack & Wijffels, 2010) over the oceans. Another possible explanation could be increased coastal runoff, either riverine or from glacial meltwater, although much of such an increase would likely be confined to the shelf and the slope in the Alaska Coastal Current (Royer & Grosch, 2006). Reduced flows of warm, salty North Pacific water are another possibility. Finally, since salinity and density are so tightly linked in the basin, a change in the gyre strength could also induce some change in the upper ocean salinity through vertical heave of isopycnals. However, isopycnal heave would not account for observed mixed-layer freshening (Figure 9).

Acknowledgments

Argo data were collected and made freely available by the International Argo Program and the national programs that contribute to it. (http://www.argo.ucsd.edu, http://argo.jcommops.org). The Argo Program is part of the Global Ocean Observing System. D. Giglio (personal communication, 2017) generously provided the code we used to make an objective map of nondivergent stream function from Argo float parking depth displacement data. Comments from Howard Freeland and an anonymous reviewers\ helped to improve the manuscript. Data used in this study can be accessed at the URLs found in section 2. G.C.J. is supported by the Climate Observation Division, Climate Program Office, National Oceanic and Atmospheric Administration (NOAA), U.S. Department of Commerce and NOAA Research. Pacific Marine Environmental Laboratory contribution 4706.

References

Amante, C., & Eakins, B. W. (2009). ETOPO1 arc-minute global relief model: Procedures, data sources, and analysis (NOAA Tech. Mem. NESDIS NGDC-24, 19 pp.). Boulder, CO: NOAA/NESDIS, National Geophysical Center, Marine Geology and Geophysics Division.

Bond, N. A., Overland, J. E., & Turet, P. (1994). Spatial and temporal characteristics of the wind forcing of the Bering Sea. *Journal of Climate*, *7*(7), 1119–1130. https://doi.org/10.1175/1520-0442(1994)007<1139:SATCOT>2.0.CO;2

Bretherton, F. P., Davis, R. E., & Fandry, C. B. (1976). A technique for objective analysis and design of oceanographic experimented applied to MODE–73. *Deep Sea Research Oceanographic Abstracts*, *23*, 559–582. https://doi.org/10.1016/0011-7471(76)90001-2

Chen, S. M., & Firing, E. (2006). Currents in the Aleutian Basin and subarctic North Pacific near the dateline in summer 1993. *Journal of Geophysical Research*, *111*, C03001. https://doi.org/10.1029/2005JC003064

Cleveland, W. S., & Devlin, S. J. (1988). Locally weighted regression: An approach to regression-analysis by local fitting. *Journal of the American Statistical Association*, *83*(403), 596–610. https://doi.org/10.2307/2289282

Cokelet, E. D., Schall, M. L., & Dougherty, D. M. (1996). ADCP-referenced geostrophic circulation in the Bering Sea basin. *Journal of Physical Oceanography*, *26*(7), 1113–1128. https://doi.org/10.1175/1520-0485(1996)026<1113:ARGCIT>2.0.CO;2

Durack, P. J., & Wijffels, S. E. (2010). Fifty-year trends in global ocean salinities and their relationship to broad-scale warming. *Journal of Climate*, *23*(16), 4342–4362. https://doi.org/10.1175/2010JCLI3377.1

Gille, S. T. (2003). Float observations of the Southern Ocean. Part I: Estimating mean fields, bottom velocities, and topographic steering. *Journal of Physical Oceanography*, *33*(6), 1167–1181. https://doi.org/10.1175/1520-0485(2003)033<1167:FOOTSO>2.0.CO;2

Holte, J., & Talley, L. (2009). A new algorithm for finding mixed layer depths with applications to Argo data and Subantarctic mode water formation. *Journal of Atmospheric and Oceanic Technology*, *26*(9), 1920–1939. https://doi.org/10.1175/2009JTECHO543.1

IOC, SCOR, & IAPSO (2010). The international thermodynamic equation of seawater-2010: Calculation and use of thermodynamic properties. In *Intergovernmental oceanographic commission, manuals and guides* (No. 56, 196 pp.) [English]. Paris, France: UNESCO.

Johnson, G. C., Stabeno, P. J., & Riser, S. C. (2004). The Bering Slope Current system revisited. *Journal of Physical Oceanography*, *34*(2), 384–398. https://doi.org/10.1175/1520-0485(2004)034<0384:TBSCSR>2.0.CO;2

Ladd, C. (2014). Seasonal and interannual variability of the Bering Slope Current. *Deep-Sea Research Part II: Topical Studies in Oceanography*, *109*, 5–13. https://doi.org/10.1016/j.dsr2.2013.12.005

Large, W. G., & Yeager, S. G. (2009). The global climatology of an interannually varying air-sea flux data set. *Climate Dynamics*, *33*(2–3), 341–364. https://doi.org/10.1007/s00382-008-0441-3

Lebedev, K., Yoshinari, H., Maximenko, N. A., & Hacker, P. W. (2007). *Yomaha'07: Velocity data assessed from trajectories of Argo floats at parking level and at the sea surface* (Tech. Note 4(2), p. 16). Honolulu, Hawai'i: International Pacific Research Center, University of Hawai'i.

Overland, J. E., Wang, M., Wood, K. R., Percival, D. B., & Bond, N. A. (2012). Recent Bering Sea warm and cold events in a 95-year context. *Deep Sea Research II: Topical Studies in Oceanography*, *65–70*, 6–13. https://doi.org/10.1016/j.dsr2.2012.02.013

Panteleev, G., Yaremchuk, M., Stabeno, P. J., Luchin, V., Nechaev, D. N., & Kikuchi, T. (2011). Dynamic topography of the Bering Sea. *Journal of Geophysical Research*, *116*, C05017. https://doi.org/10.1029/2010JC006354

Panteleev, G. G., Stabeno, P., Luchin, V. A., Nechaev, D. A., & Ikeda, M. (2006). Summer transport estimates of the Kamchatka Current derived as a variational inverse of hydrophysical and surface drifter data. *Geophysical Research Letters*, *33*, L09609. https://doi.org/10.1029/2005GL024974

Reed, R. K. (1995). On the variable subsurface environment of fish stocks in the Bering Sea. *Fisheries Oceanography*, *4*(4), 317–323. https://doi.org/10.1111/j.1365-2419.1995.tb00076.x

Reed, R. K., Khen, G. V., Stabeno, P. J., & Verkhunov, A. V. (1993). Water properties and flow over the deep Bering Sea Basin, Summer 1991. *Deep Sea Research Part I: Oceanographic Research Papers*, *40*(11–12), 2325–2334. https://doi.org/10.1016/0967-0637(93)90107-E

Royer, T. C., & Grosch, C. E. (2006). Ocean warming and freshening in the northern Gulf of Alaska. *Geophysical Research Letters*, *33*, L16605. https://doi.org/10.1029/2006GL026767

Stabeno, P. J., Duffy-Anderson, J. T., Eisner, L. B., Farley, E. V., Heintz, R. A., & Mordy, C. A. (2017). Return of warm conditions in the Bering Sea. *PLoS One*, *12*(9), e0185464. https://doi.org/10.1371/journal.pone.0185464

Stabeno, P. J., Kachel, D. G., Kachel, N. B., & Sullivan, M. E. (2005). Observations from moorings in the Aleutian Passes: Temperature, salinity and transport. *Fisheries Oceanography*, *14*, 39–54. https://doi.org/10.1111/j.1365-2419.2005.00362.x

Stabeno, P. J., Kachel, N. B., Moore, S. E., Napp, J. M., Sigler, M., Yamaguchi, A., & Zerbini, A. N. (2012). Comparison of warm and cold years on the southeastern Bering Sea shelf and some implications for the ecosystem. *Deep Sea Research Part II: Topical Studies in Oceanography*, *65–70*, 31–45. https://doi.org/10.1016/j.dsr2.2012.02.020

Stabeno, P. J., Ladd, C., & Reed, R. K. (2009). Observations of the Aleutian North Slope Current, Bering Sea, 1996–2001. *Journal of Geophysical Research*, *114*, C05015. https://doi.org/10.1029/2007JC004705

Thorpe, S. A. (1977). Turbulence and mixing in a Scottish Loch. *Philosophical Transactions of the Royal Society of London A*, *286*, 125–181. https://doi.org/10.1098/rsta.1977.0112

Ueno, H., & Yasuda, I. (2000). Distribution and formation of the mesothermal structure (temperature inversions) in the North Pacific subarctic region. *Journal of Geophysical Research*, *105*(C7), 16885–16897. https://doi.org/10.1029/2000JC900020

Wirts, A. E., & Johnson, G. C. (2005). Recent interannual upper ocean variability in the deep southeastern Bering Sea. *Journal of Marine Research*, *63*(2), 381–405. https://doi.org/10.1357/0022240053693725

Woodgate, R. A., Weingartner, T. J., & Lindsay, R. (2012). Observed increases in Bering Strait oceanic fluxes from the Pacific to the Arctic from 2001 to 2011 and their impacts on the Arctic Ocean water column. *Geophysical Research Letters*, *39*, L24603. https://doi.org/10.1029/2012GL054092